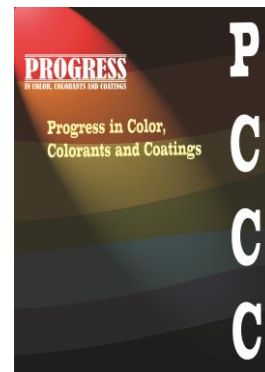


Accepted Manuscript

**Title: Multifunctional Epoxy Coatings with GA-Functionalized MWCNTs: Corrosion Resistance and Thermo-Mechanical Performance for Steel Protection**



**Authors:** Z. Asadi Sajed, M. Rostami, M. Ganjaee Sari, B. Ramezanzadeh, M. S. Ghorashi

Manuscript number: **PCCC-2510-1462**

To appear in: Progresss in Color, Colorants and Coatings

Received: 29 September 2025

Final Revised: 11 November 2025

Accepted: 12 November 2025

Please cite this article as:

Z. Asadi Sajed, M. Rostami, M. Ganjaee Sari, B. Ramezanzadeh, M. S. Ghorashi, Multifunctional Epoxy Coatings with GA-Functionalized MWCNTs: Corrosion Resistance and Thermo-Mechanical Performance for Steel Protection, Prog. Color, Colorants, Coat., 19 (2026) XX-XXX.

DOI: 10.30509/pccc.2025.167700.1462

This is a PDF file of the unedited manuscript that has been accepted for publication. The manuscript will undergo copyediting, typesetting, and review of the resulting proof before it is published in its final form

**Multifunctional Epoxy Coatings with GA-Functionalized MWCNTs: Corrosion  
Resistance and Thermo-Mechanical Performance for Steel Protection**

Z. Asadi Sajed <sup>a</sup>, M. Rostami <sup>a\*</sup>, M. Ganjaee Sari <sup>a</sup>, B. Ramezanzadeh <sup>b</sup>, M.S. Ghorashi

<sup>a\*\*</sup>

<sup>a</sup> Department of Nanomaterials and Nanocoatings, Institute for Color Science and  
Technology, P.O. Box 16765-654, Tehran, Iran

<sup>b</sup> Department of Surface Coatings and Corrosion, Institute for Color Science and  
Technology, P.O. Box 16765-654, Tehran, Iran

Email: \* rostami-m@icrc.ac.ir; \*\* ghorashi-ms@icrc.ac.ir

**Abstract**

Amine-functionalized multi-wall carbon nanotubes (MWCNTs-NH<sub>2</sub>) were employed as nanocarriers for gallic acid (GA), a green corrosion inhibitor, to develop multifunctional epoxy nanocomposites for steel protection in saline environments. GA was effectively immobilized onto MWCNTs-NH<sub>2</sub> to attain both active corrosion inhibition and enhanced barrier performance. Electrochemical impedance spectroscopy and polarization performed after 72 hours of immersion in saline solution indicated a ~91% increase in total resistance and a ~ 47% decrease in corrosion current density for the optimized MWCNT-NH<sub>2</sub>/GA system compared to uninhibited samples. Epoxy coatings containing 0.15 wt.% of the synthesized nanocomposites demonstrated active protection in damaged regions, as confirmed by EIS and salt-spray testing. Following 24 hours of exposure to saline solution, the total resistance of the epoxy coating with 50% GA loading increased by ~560% relative to the bare samples. Furthermore, the  $\log|Z|_{10\text{ mHz}}$  value, which serves

as a suitable measure of self-healing ability in the scratched region, increased to  $\sim 4.8 \text{ k}\Omega\cdot\text{cm}^2$ . While it showed a notable decrease for uncoated epoxy, falling below  $0.4 \text{ k}\Omega\cdot\text{cm}^2$ . These coatings also exhibited significantly improved adhesion under both dry and wet conditions. Adhesion loss for the epoxy coating containing the optimal 50% GA loading was  $\sim 6\%$ . Notably, cathodic disbondment was reduced by 50% and 42% relative to neat epoxy and MWCNTs-NH<sub>2</sub>-containing epoxy coatings, respectively, in the 50% GA-loaded formulation. Furthermore, Thermo-mechanical analysis confirmed enhanced toughness reinforcement. Overall, the synergistic barrier effect of MWCNTs-NH<sub>2</sub> and the controlled release of gallate ions provide a promising strategy for durable, self-healing corrosion protection in harsh environments.

**Keywords:** Epoxy nanocomposites; Gallic acid-functionalized MWCNTs; Self-healing corrosion protection; Thermo-mechanical properties.

## 1. Introduction

Corrosion remains a pervasive scientific and economic challenge, drawing sustained attention from researchers, industrial stakeholders, and policy makers. Its impact on infrastructure and productivity has elevated corrosion control to a strategic priority in many nations. According to the World Corrosion Organization, annual corrosion-related losses in industrialized countries amount to 2-4% of their gross national product [1], underscoring the urgent need for effective mitigation strategies.

Applying organic polymer coatings, such as epoxy, to metal surfaces is one of the easiest and most affordable ways to enhance their corrosion resistance. Epoxy coatings typically

mitigate the corrosion of metal substrates exposed to electrolytes through two main mechanisms. Firstly, they function as a physical barrier that limits the penetration of detrimental species. Secondly, they can act as a storage medium for corrosion inhibitors, which help protect the steel surface from aggressive agents like chloride ions. While epoxy coatings are widely used for their affordability and ease of application, their long-term performance is often compromised under aggressive service conditions. The inherent porosity and limited adhesion of epoxy resins restrict their durability, especially in harsh environments where polymer degradation accelerates. To overcome these limitations, researchers have explored incorporating nanomaterials-such as  $\text{SiO}_2$ , graphene, carbon nanotubes (CNTs), nanoclays, and phosphates-into epoxy matrices to enhance barrier properties, mechanical strength, and corrosion resistance [2-6]..

CNT is a well-known carbon-based nanomaterial that has been successfully applied as an anticorrosive material in polymer composites. CNTs offer high aspect ratios with a hollow cylindrical structure, excellent conductivity, outstanding chemical and thermal stability, and tunable surface chemistry, making them ideal candidates for reinforcing polymer coatings [7-9]. Functionalization with amine groups (MWCNTs- $\text{NH}_2$ ) enhances dispersion and interfacial bonding by increasing surface polarity and introducing hydrogen-bonding sites, thereby improving their compatibility with polar polymers (e.g., epoxies, polyamides), reducing agglomeration, and allowing more uniform dispersion in the matrix [10, 11]. Jeon [12] explored the advantageous impacts of MWCNTs application in epoxy coatings regarding hydrophobicity and water transport behavior, and thus on corrosion resistance. Liu [6] developed MWCNTs- $\text{CeO}_2$ @polydopamine by incorporating  $\text{CeO}_2$  onto MWCNTs through a straightforward one-pot method that

included polydopamine modification. By integrating MWCNTs-CeO<sub>2</sub>@polydopamine within waterborne epoxy, improved corrosion protection was achieved. The combination of the extended and obstructed diffusion pathways created by MWCNTs, along with the corrosion-inhibition properties of CeO<sub>2</sub>, provided the composite coating with remarkable anticorrosion performance in saline solution. Gharemani [13] developed an innovative corrosion inhibitor nanocarrier by surface-modifying MWCNTs with mussel-inspired polydopamine, chitosan, and zinc cations. The incorporation of this nanocomposite into the epoxy coating imparted exceptional barrier properties and ensured consistent corrosion inhibition. Nayak [13] synthesized the functionalized multi-walled carbon nanotube/polyindole, designed to enhance the anticorrosion effectiveness of the epoxy matrix. The even distribution of the nanocomposite, along with the extended pathway for corrosive electrolytes, renders it an outstanding coating for anticorrosion purposes. Madhusudhana [14, 15] formulated a filler material with MWCNT-incorporated nanocapsules, which was later blended with phenol novolac resin. The phenol novolac resin with 0.3 wt.% MWCNT/nanocapsules showed a marked increase in hydrophobicity and demonstrated improved long-term anticorrosion efficiency and self-healing properties in saline solution.

Gallic acid (GA) is a naturally occurring polyphenolic compound recognized for its antioxidant properties, naturally present in various plants and fruits, including tea leaves, oak bark, and berries. Its molecular composition features an aromatic ring, one carboxyl group, and three phenolic hydroxyl groups. The trihydroxyphenyl configuration of GA enables it to effectively adhere to substrate surfaces through both covalent and noncovalent interactions. GA can effectively graft onto metallic surfaces while

preserving its redox activity. It can function as a coupling agent or an interfacial modifier [14, 15].

Additionally, its interaction with metal oxides existing on the steel surface leads to the formation of complexes that enhance surface roughness, potentially facilitating improved mechanical interlocking [16]. Consequently, GA can enhance the adhesion of films, thereby improving their barrier properties and passivation [17, 19]. Recent research has shown that GA can serve as an effective corrosion inhibitor. This is due to its oxygen-based groups interacting with the surface oxide layer via hydrogen bonding or coordination bonds [5, 20, 21]. Liu [5] developed acrylic latex composite coatings reinforced with gallic acid-modified montmorillonite, resulting in improved mechanical properties, such as hardness and wear resistance, as well as enhanced thermal stability. Additionally, the anticorrosive properties were enhanced through barrier and interface passivation. Zhao [22] employed a ZIF nanosheet framework as a vehicle for the GA corrosion inhibitor, thereby improving the physical barrier properties of the waterborne epoxy coating through its distinctive two-dimensional structure. PEG was used to form a PEG-GA complex layer, firmly anchoring GA to the nanosheet surface.

This study aims to develop a multifunctional corrosion inhibitor by impregnating GA, a polyphenolic compound with antioxidant activity, onto MWCNTs-NH<sub>2</sub> and integrating the resulting nanocomposite into epoxy coatings. The significant innovation presented in this study, relative to prior research, is the exploration of the MWCNT-NH<sub>2</sub>/GA nanocomposite as an inorganic inhibitor in solution, along with its merits for epoxy coatings, providing a self-healing, anticorrosive coating with superior cathodic delamination resistance and adhesion. Structural characterization was performed using

FE-SEM, EDS/Mapping, FTIR, Raman spectroscopy, and TGA. The anticorrosion effectiveness, adhesion behavior, and self-healing ability of the coatings were evaluated using electrochemical methods (polarization and EIS), salt spray testing, pull-off adhesion testing, and cathodic delamination studies. Thermo-mechanical properties were also assessed using dynamic mechanical thermal analysis (DMTA) to determine the coatings' durability under thermal stress. GA provided active corrosion protection by forming a thin protective layer on the metal surface, effectively controlling corrosion reactions and imparting self-healing capability to the epoxy coating. GA functions as a free radical scavenger, thereby inhibiting the rapid generation of these species in the cathodic areas and reducing the cathodic separation phenomenon. Regarding the inhibition potential of GA and its effective interaction with MWCNT, the results show a significant enhancement in the corrosion resistance of the epoxy coating.

**Table 1** presents a comprehensive list of all the abbreviations used in this research.

Abbreviation	Explanation	Abbreviation	Explanation
MWCNT	Multiwall Carbon nanotubes	EEC	Equivalent electric circuit
CNTs	Carbon nanotubes	$\eta$	Protection efficiency
GA	Gallic acid	DI	Delamination index
EIS	Electrochemical impedance spectroscopy	$R_s$	Solution resistance
FE-SEM	Field Emission Scanning Electron Microscope	$R_f$	Resistance of the generated films
EDS	Energy dispersive X-ray spectroscopy	$R_{ct}$	Charge transfer resistance
FTIR	Fourier transform infrared	$R_t$	Total resistance
TGA	Thermogravimetry analysis	$Q_f$	Constant phase element of the generated film

DTG	derivative thermogravimetry	$Y_{0,f}$	Non-ideal capacitance of the generated film
DTA	Differential thermal analysis	$n_f$	Phase shift of the generated film
%TG	%Weight loss	$Q_{dl}$	Constant phase element of the double layer
DMTA	Dynamic Mechanical Thermal Analysis	$Y_{0,dl}$	Non-ideal double-layer capacitance
$i_{corr}$	Corrosion current density	$n_{dl}$	Double-layer phase shift
$E_{corr}$	Corrosion potential		
$\beta_a$	Anodic Tafel slope		
$\beta_c$	Cathodic Tafel slope		

## 2. Experimental

### 2.1. Materials

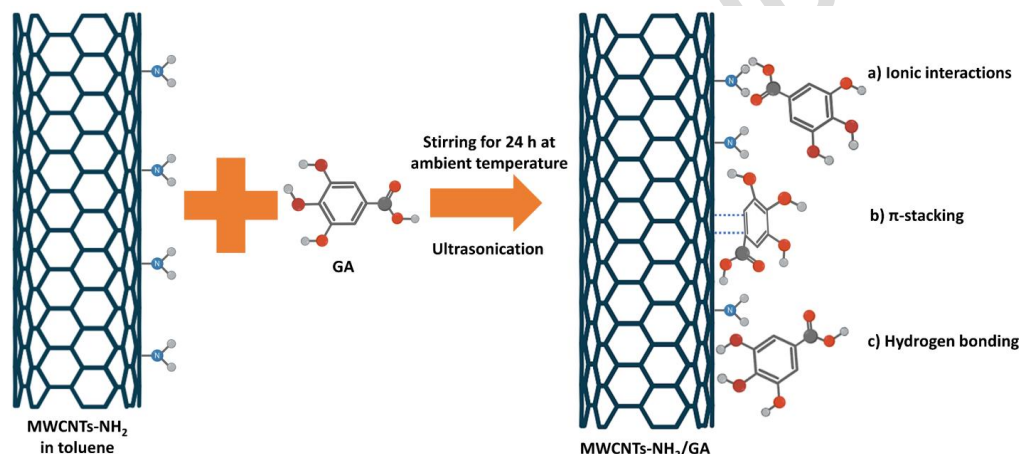
MWCNT-NH<sub>2</sub> (Purity:>95%, Content of -NH<sub>2</sub>: 0.45 wt.%, 1–10  $\mu$ m, and wall number of 3–15) was obtained from Nanostartech (Iran). Epoxy resin (EEW: 434 g/eq, Epiran-01X75) and polyamide hardener (Crayamid115) were provided by Saba Shimi Company (Iran). Gallic acid (GA) and toluene were obtained from Sigma-Aldrich. Acetone and NaCl were obtained from Mojallali Co., an Iranian supplier. Low-carbon steel (ST12) coupons, measuring 10 cm  $\times$  8 cm  $\times$  0.1 cm, were obtained from FooladMobarakeh Co. (Iran).

### 2.2. Synthesis of GA-modified MWCNTs-NH<sub>2</sub>

Figure 1 illustrates the surface modification process of MWCNT-NH<sub>2</sub> with GA and the interactions involved. To achieve stable dispersion of MWCNT-NH<sub>2</sub> and GA, 0.1 g of



MWCNT-NH<sub>2</sub> was added to 100 mL of toluene with varying GA weight percentages (0, 25, 50, and 75 weight %). The obtained solutions were magnetically stirred at room temperature for 24 h, followed by ultrasonication at 150 kW for 5 minutes. The obtained samples will thereafter be referred to as MWCNT-NH<sub>2</sub>, MWCNT-NH<sub>2</sub>/GA25%, MWCNT-NH<sub>2</sub>/GA50%, and MWCNT-NH<sub>2</sub>/GA75%. The washing process of MWCNT-NH<sub>2</sub>/GA was performed by ultracentrifugation and redispersion in toluene 3 times. GA can form a carboxylate-ammonium ionic bond, hydrogen bonds, and  $\pi$ - $\pi$  interactions with MWCNTs-NH<sub>2</sub>.



**Figure 1.** Schematic representation of the immobilization process of the GA inhibitor on NH<sub>2</sub>-MWCNTs and the involved interactions between MWCNTs-NH<sub>2</sub> and GA.

### 2.3. Electrolytes and sample preparation

To prepare the steel coupons for testing and coating, ST1 coupons were cleaned with acetone. Afterwards, they were polished with grit carbide papers, and the polished samples were stored under humidity-free conditions.

To prepare the epoxy coatings, MWCNT-NH<sub>2</sub>/GA was added to toluene at a volume ratio of 1:10. The mixture was sonicated at 150 kW for 5 min, then added to the epoxy resin.

The resin and solvent mixtures were again sonicated for 8 min in an ice-water bath to disperse the particles in the resin completely. Then, each mixture was stirred for 24 h using a laboratory mixer to disperse the nanoparticles in the epoxy resin uniformly. Afterwards, the polyamide curing agent was blended at a mass ratio of 1.3:1 (resin: hardener). The quantity of MWCNT- NH<sub>2</sub>/GA was determined to yield a final weight percentage of nanoparticles in the dry epoxy/polyamide composite of 0.15%. The coatings were applied to steel samples measuring 100 mm × 80 mm × 3 mm using a Braive 35200016 film coater. The samples were stored in a clean room at 25 °C for 4 days. The curing was performed by heating in an oven for 3 hours at 80 °C. The samples were named EP-NH<sub>2</sub>-MWCNT/GA, EP-NH<sub>2</sub>-MWCNT/GA25%, EP-MWCNT-NH<sub>2</sub>/GA50% and EP-MWCNT-NH<sub>2</sub>/GA75% according to the particles used in the composites. The reference coating without particles was also named EP. The coating thickness for the pull-off, salt spray, and cathodic delamination studies was 350 µm, whereas for the EIS analyses, it was 100 µm.

#### 2.4. Characterization techniques

The surface composition of the nanoparticles was investigated using an FTIR device manufactured by PerkinElmer in the wavelength range of 4000-500 cm<sup>-1</sup>. FE-SEM (Tescan Mira3-LMU) images were acquired at various magnifications to examine the sample morphology. Additionally, EDS/mapping analysis was employed to ascertain the elemental composition of the immersed samples for an in-depth study. The samples were exposed to bare and NH<sub>2</sub>-MWCNT/GA-containing electrolytes for 48 hours to obtain the captures. The amount of surface functional groups on the MWCNTs-NH<sub>2</sub> was evaluated

by a Perkin-Elmer Thermogravimetric Analyzer Pyris 1 TGA model (USA). Heating was carried out from 30 to 600 °C at a rate of 10 °C/min. Confocal Raman microscopy (Horiba XploraPlus, France) was used better to characterize the structures of modified and unmodified carbon nanotubes. The device's experimental data were fitted using OriginPro 2016. The Tritec 2000 type dynamic mechanical thermal analysis (DMTA) instrument was used to investigate the mechanical properties of free-standing MWCNT-NH<sub>2</sub>/GA nanocomposite films. The DMTA procedure was carried out at 1 Hz, over the temperature range 243-433 K, and at a heating rate of 278 K min<sup>-1</sup>.

To assess the anticorrosion capabilities of the MWCNT-NH<sub>2</sub>/GA nanocomposite, electrochemical testing techniques were utilized. The anticorrosion mechanism was analyzed using potentiodynamic polarization curves, and the samples' resistance was evaluated using EIS. The electrochemical arrangement included a standard three-electrode setup: a platinum electrode as the counter, a Calomel electrode as the reference, and the metal sample as the working electrode, all connected to an IviumCompactstat device. The coupons for testing were submerged in a 3.5 wt.% NaCl solution, with an exposed area of 1 cm<sup>2</sup>, considering different exposure durations. The data collected from the experiments were analyzed using Zsim software, yielding a chi-squared ( $\chi$ ) value of less than 0.01. Tafel curves were generated by sweeping the potential range of +250 mV to -250 mV at a scan rate of 1 mV/s. Additionally, Nyquist and Bode plots were obtained by varying the frequency from 0.01 Hz to 10,000 Hz with a scan rate of 10 mV/s.

The adhesion strength of the coatings was assessed under both wet and dry conditions using DeFelsko equipment and a pull-off test. For the wet adhesion evaluation, the coated samples were placed in a salt spray chamber for 7 days before analysis. A 5% NaCl

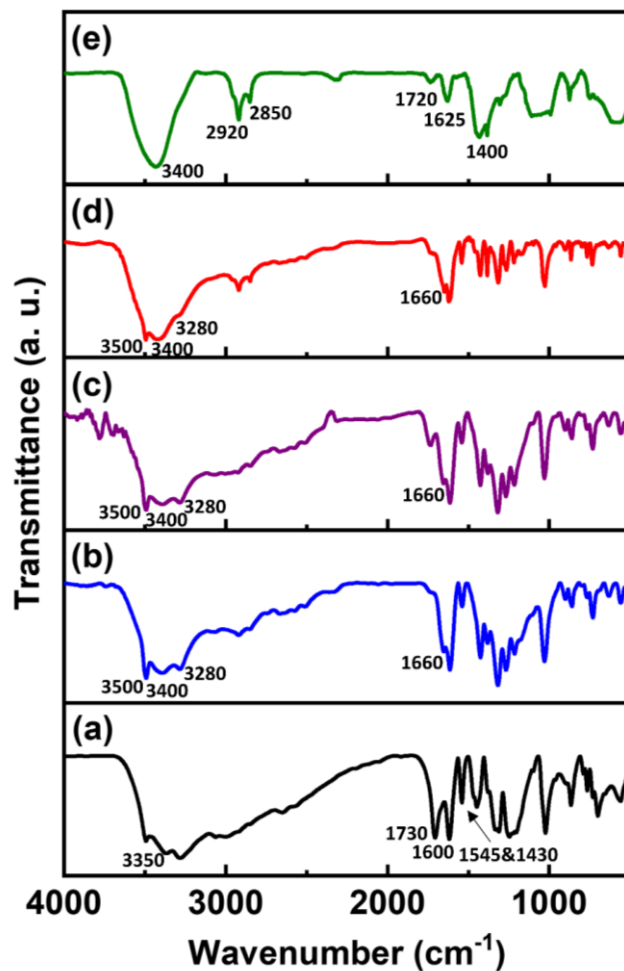
solution was frequently showered onto the samples within a controlled chamber maintained at 40 °C.

### 3. Results and Discussion

#### 3.1. Characterization of MWCNT-NH<sub>2</sub>/GA

FTIR spectra of GA, MWCNT-NH<sub>2</sub>, and MWCNT-NH<sub>2</sub>/GA were examined to confirm the surface modification of MWCNT-NH<sub>2</sub> with GA (Figure 2). The broad and strong band at about 3200 to 3500 cm<sup>-1</sup> corresponds to the vibrations of the OH and carboxylic OH groups in GA and MWCNT-NH<sub>2</sub>/GA. Typical aromatic bands can be observed at 1617-1608 cm<sup>-1</sup> (C=C stretching vibrations), 1559–1540 cm<sup>-1</sup> (C-C stretching vibrations), 2920 and 2850 cm<sup>-1</sup> (the stretching vibration of the aromatic C-H bond), which are common among GA and MWCNTs [23, 24]. The peaks in the ~1300-1200 cm<sup>-1</sup> region can be ascribed to the C-O stretching, and O-H bending (carboxylic OH) vibrations appear at 1410-1440 cm<sup>-1</sup> of GA and MWCNT-NH<sub>2</sub>/GA. A strong, sharp peak at ~1730-1700 cm<sup>-1</sup> can be assigned to the carbonyl (C=O) stretching vibration from the carboxyl group [25]. In the FTIR spectrum of MWCNT-NH<sub>2</sub>, absorption bands in the range of 3500-3250 cm<sup>-1</sup> appear due to symmetric and asymmetric stretching modes of amines. The peak at ~1400 cm<sup>-1</sup> is attributed to the C-N stretching vibration or N-H bending of MWCNT-NH<sub>2</sub>, which is also present in MWCNT-NH<sub>2</sub>/GA [26, 27]. In the spectra of MWCNT-NH<sub>2</sub>/GA, the carbonyl group at ~1730-1700 cm<sup>-1</sup> has disappeared. Instead, a new peak ascribed to amide carbonyl groups has emerged at ~1660 cm<sup>-1</sup> in MWCNT-NH<sub>2</sub>/GA samples, indicating that amine groups on MWCNT-NH<sub>2</sub> react with the carboxylate group of GA to form amide groups. Three strong peaks at ~3500, 3400, and

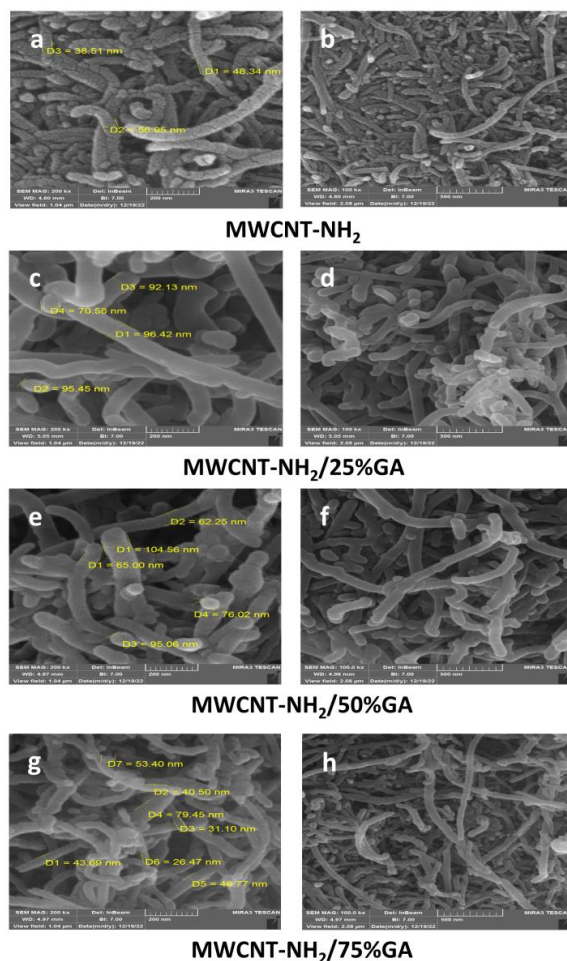
3282  $\text{cm}^{-1}$  indicate N-H stretching of an amide [28]. The results show that the spectra of MWCNT-NH<sub>2</sub>/GA exhibit peaks corresponding to both MWCNT-NH<sub>2</sub> and GA. However, there are some overlaps between the peaks of MWCNTs and GA. These findings corroborate the successful surface modification of MWCNTs with GA.



**Figure 2.** FTIR spectra of (a) GA, (b) MWCNT-NH<sub>2</sub>-25% GA, (c) MWCNT-NH<sub>2</sub>-50% GA, (d) MWCNT-NH<sub>2</sub>-75% GA, and (e) MWCNT-NH<sub>2</sub>.

FE-SEM images were used to examine the morphology, changes in nanotube diameter, and the relative positions of MWCNTs. Figure 3 demonstrates FE-SEM images of MWCNT-NH<sub>2</sub>(a, b), MWCNT-NH<sub>2</sub>/25% GA (c, d), MWCNT-NH<sub>2</sub>/50% GA (e, f), and

MWCNT-NH<sub>2</sub>/75%GA (g, h). The maximum diameters for MWCNT-NH<sub>2</sub>, MWCNT-NH<sub>2</sub>/GA25%, MWCNT-NH<sub>2</sub>/GA50%, and MWCNT-NH<sub>2</sub>/GA75% were 56.95, 96.42, 104.56, and 79.45 nm, respectively. The diameter of MWCTs containing the GA inhibitor is obviously greater than that of the sample without the inhibitor, confirming the successful modification of MWCNTs with GA. FE-SEM images also clearly demonstrate the increased diameter of the nanotubes upon GA surface modification up to 50% GA loading. The tube diameter distribution of MWCNT-NH<sub>2</sub> has also improved following GA surface modification, which proves the superior coating homogeneity. Given the maximum diameter observed in MWCNT-NH<sub>2</sub>/GA50%, it can be inferred that GA exhibited a greater capacity to react with MWCNTs in this sample. The decrease in diameter in MWCNT-NH<sub>2</sub>/GA75% can be attributed to incomplete GA absorption on MWCNTs. The FESEM images clearly show that the relative distance among the MWCNTs-NH<sub>2</sub> in MWCNT-NH<sub>2</sub>/GA50% is more pronounced than in the other samples, indicating that GAs significantly contribute to improved dispersion and reduced agglomeration of MWCNTs-NH<sub>2</sub>.

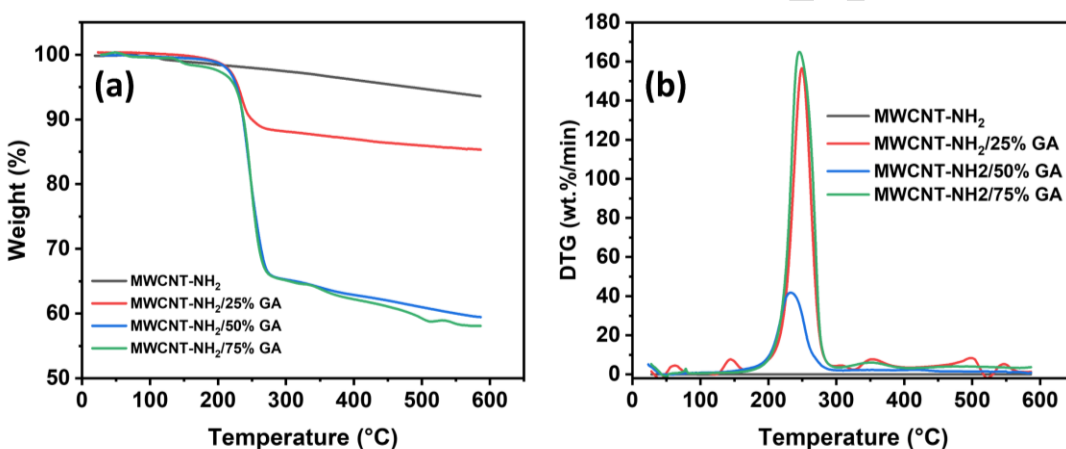


**Figure 3.** FE-SEM images of MWCNT-NH<sub>2</sub> (a,b), MWCNT-NH<sub>2</sub>/25%GA (c,d), MWCNT-NH<sub>2</sub>/50%GA (e,f), and MWCNT-NH<sub>2</sub>/75%GA (g,h).

The thermal analysis results for MWCNT-NH<sub>2</sub>/x% GA (x = 0, 25, 50, 75) are depicted in Figure 4. Figure 4a displays the thermogravimetric results of the different samples. For MWCNT-NH<sub>2</sub>, the total weight loss (~7 %) achieved at a constant rate is ascribed to the elimination of both adsorbed and crystalline water and surface-adsorbed NH<sub>2</sub> functional groups. By comparing the graphs of the GA-modified samples with the bare MWCNT-NH<sub>2</sub> sample, a change in the graph's behavior is evident in the temperature range of 200-275 °C. The sudden decrease in the weight of the sample compared to the initial weight (%TG) signifies the thermal decomposition of surface-adsorbed gallate ions [29]. As

anticipated, the percentage of weight variation in the samples correlates with the percentage of GA present in the structure (e.g., 11% for MWCNT-NH<sub>2</sub>/25% GA and ~33% for MWCNT-NH<sub>2</sub>/50% GA and MWCNT-NH<sub>2</sub>/75% GA).

Furthermore, the derivative thermogravimetry (DTG) results (Figure 4b) corroborate the abrupt weight changes in the MWCNT-NH<sub>2</sub>/x% GA (x = 25, 50, 75) samples within the temperature range of 200-275 °C, demonstrating the effective modification of MWCNT-NH<sub>2</sub> by GA. Overall, the various thermal analysis results validate the existence of GA in the anticipated weight sequence within the system.

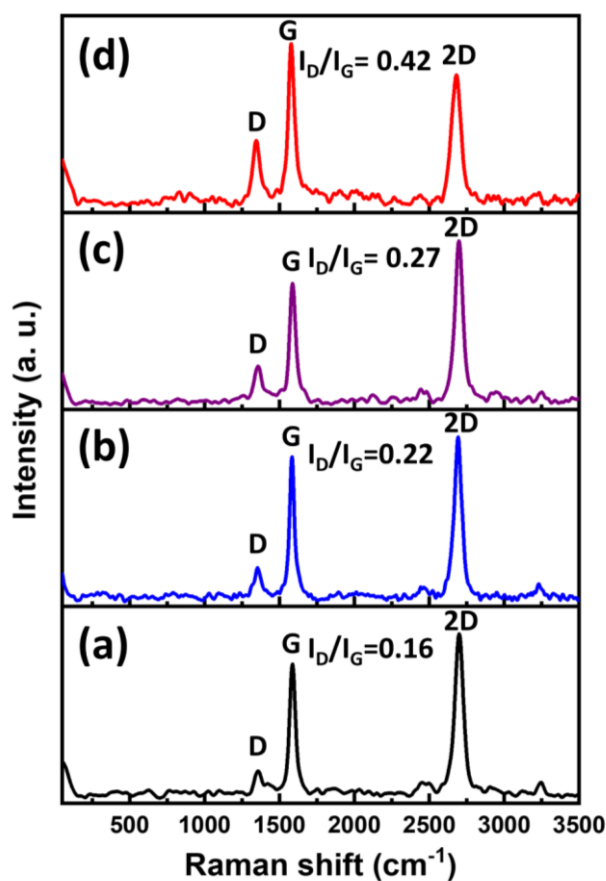


**Figure 4 .** Thermal analysis results for MWCNT-NH<sub>2</sub>/x% GA (x= 0, 25, 50, 75)(a) Thermogravimetry analysis (TGA) and (b) derivative thermogravimetric (DTG) results.

Figure 5a-d demonstrates the Raman spectroscopy spectra for MWCNT-NH<sub>2</sub>/x% GA (x= 0, 25, 50, 75). In these spectra, the peak in the 1570-1590 cm<sup>-1</sup> region corresponds to the G band and in-plane vibrations of sp<sup>2</sup>-hybridized carbon atoms. Conversely, the peak in the region of 1340-1360 cm<sup>-1</sup> is associated with the D band and the defects of the crystal lattice of the structure. The 2D peak, which is related to the 2-photon oscillations in the structure, is located in the region of 2700-3000 cm<sup>-1</sup>. The I<sub>D</sub>/I<sub>G</sub> ratio



is a widely used metric for assessing the level of structural defects in carbon materials [30, 31]. Accordingly, the  $I_D/I_G$  ratio of MWCNT-NH<sub>2</sub> steadily escalates as the weight percentage of GA increases, implying a rise in the formation of defects due to the introduction of more functional groups on the MWCNT-NH<sub>2</sub> surface. Nevertheless, the percentage of changes is conspicuously greater for the 75% sample than for the other samples.



**Figure 5.** Raman spectra of (a) MWCNT-NH<sub>2</sub>, (b) MWCNT-NH<sub>2</sub>/25% GA, (c)/MWCNT-NH<sub>2</sub>/50% GA, (d) MWCNT-NH<sub>2</sub>/75% GA.

### 3.2. Solution phase corrosion investigation

#### 3.2.1. EIS

To evaluate the inhibition effect of MWCNT-NH<sub>2</sub>/GA on the metal surface immersed in the saline solution, EIS analysis was performed. The Nyquist and Bode plots are given in Figures 6 and 7, respectively. The electrical equivalent circuits (EEC) used for fitting are illustrated in Figure 8. The extracted EIS parameters are also presented in Table 2. The chi-square ( $\chi^2$ ) values ranged from  $10^{-3}$  to  $10^{-4}$ , indicating a reliable fit for the extraction of EIS parameters. The arc diameter in the Nyquist plot serves as a direct indicator of the coating's corrosion resistance. The largest arc diameter for the blank sample was recorded after a 2 h exposure period, after which it decreased due to the infiltration of corrosive agents into the surface. For the MW-CNT-NH<sub>2</sub> sample, the maximum arc diameter is attained after 24 hours and is estimated to be about 2500  $\Omega\cdot\text{cm}^2$ . The data also indicates that, at any given time, the arc diameters of MWCNT-NH<sub>2</sub>/GA samples exceed those of the blank samples. In the MW-CNT-NH<sub>2</sub>/GA25% sample, the arc diameters initially fluctuated, likely due to the formation and dissolution of corrosion product layers.

Nevertheless, after 24 hours, the maximum resistance is reached ( $\sim 4500\Omega\cdot\text{cm}^2$ ), followed by a downward trend. In the MWCNT-NH<sub>2</sub>/GA50% sample, a steady, gradual increase in resistance is observed over 48 hours. After 24 hours, the resistance attains approximately 23500  $\Omega\cdot\text{cm}^2$ , and by 48 hours, it exceeds 25000  $\Omega\cdot\text{cm}^2$ . This trend suggests the ongoing release of gallate ions, as the resistance remains at 23000  $\Omega\cdot\text{cm}^2$  even after 72 hours. In the MWCNT-NH<sub>2</sub>/GA75% sample, the highest resistance was observed during the first 2 hours, followed by a declining trend. This can be ascribed to suboptimal GA loading and the dissolution of the GA molecules in this sample, which fail to deliver the expected inhibitory effect.

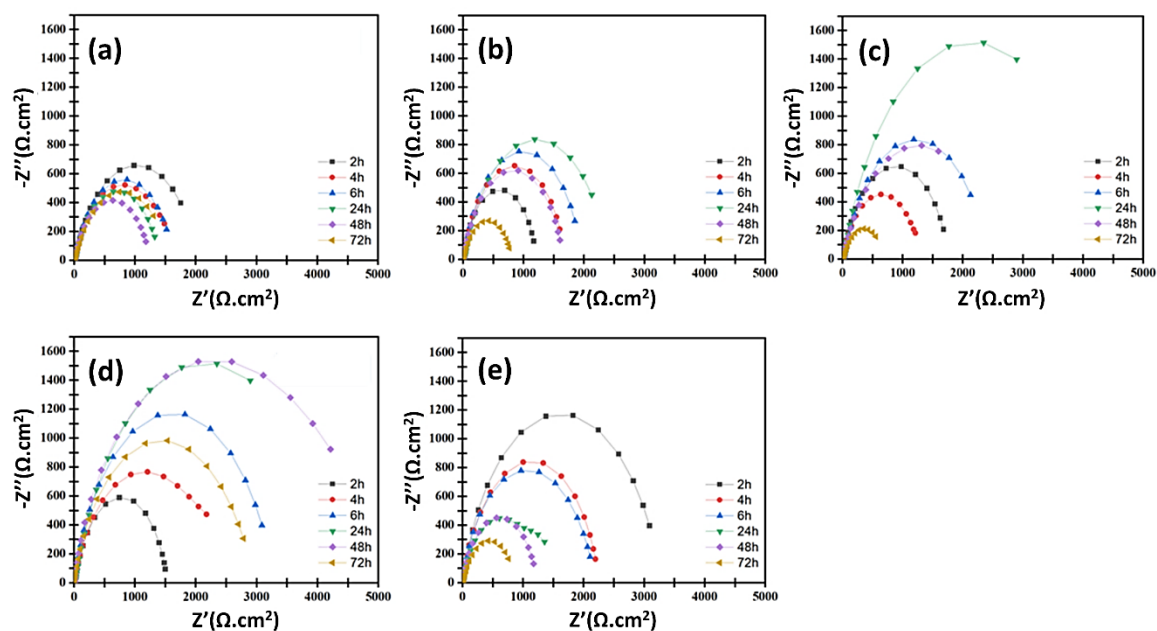
Gallate ions released from MWCNT-NH<sub>2</sub>/GA samples can interact with the substrate both physically and chemically [20, 31, 32]. Over time, GA can occupy additional active sites, leading to enhanced protection and improved anticorrosion index. Nevertheless, the overall resistance of the metal surface declined over time. This is attributed to the inhibitory layer's inadequate performance. Consequently, the corrosive solution infiltrates the supporting layer's structure, leading to its eventual destruction [20, 21].

In the phase angle diagram of the blank sample, only one relaxation time was observed. As a result, the electrochemical reactions were controlled by charge transfer, and the EEC associated with the blank sample exhibited a single time constant  $R(RQ)$ , ascribed to the porous, loosely bound corrosion products on the metal surface. Contrastingly, in the phase diagrams of MWCNT-NH<sub>2</sub>/GA, uniform films form in both cathodic and anodic regions, broadening the diagrams due to a second time constant at higher frequencies. Hence, it required an EEC featuring two time constants [33].

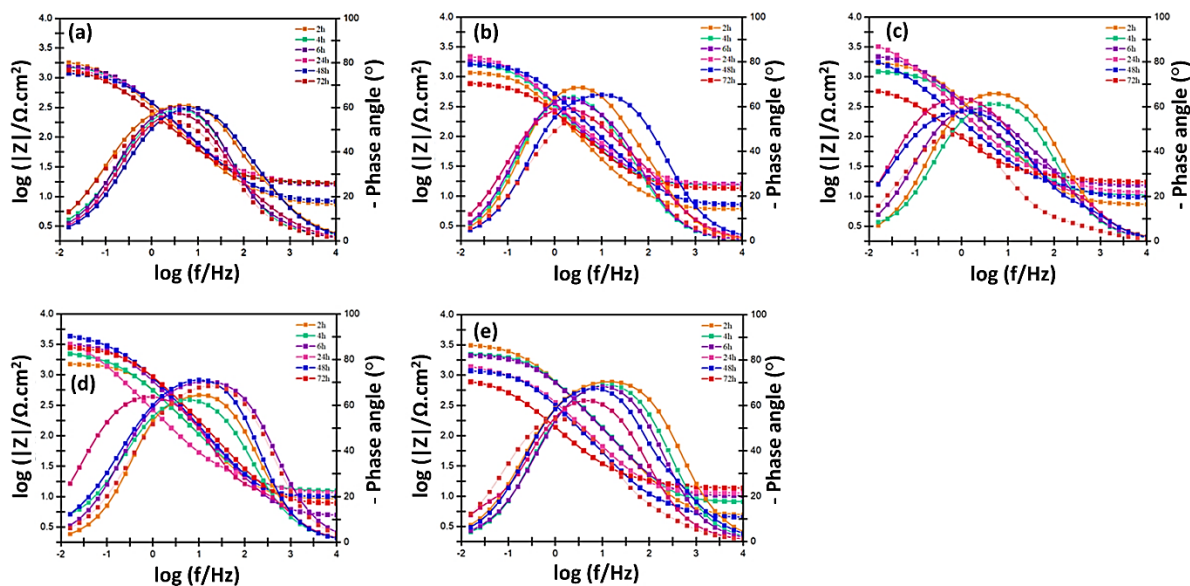
The total resistance ( $R_t$ ) of the MWCNT-NH<sub>2</sub>/X% GA samples was measured to evaluate their ability to form films and their inhibition efficiency. This parameter, which is obtained from the total of  $R_f$  and  $R_{ct}$ , is presented in Table 2. Overall, the  $R_t$  of the MWCNT-NH<sub>2</sub>/GA samples exceed those of the blank samples, with the maximum value observed for the MW-CNT-NH<sub>2</sub>/GA50%.

The impedance at low frequencies ( $\log |Z|_{10 \text{ mHz}}$ ) can also be regarded as an indicator of the overall impedance. For the blank sample,  $\log |Z|_{10 \text{ mHz}}$  did not show a significant increase over time. Conversely, this parameter has risen to 3.5 for

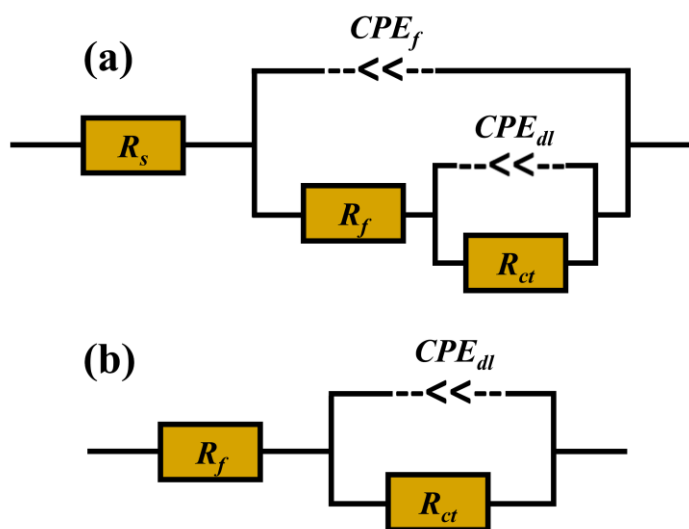
MWCNT-NH<sub>2</sub>/GA50%. This further validates the formation of a protective layer at the metal/solution interface, attributed to the release of gallate ions from MWCNT-NH<sub>2</sub>/GA and their interaction with the surface [20, 21, 32, 34]. Additionally, research findings have revealed a direct correlation between  $n$  and the uniformity of the metal surface in corrosive environments [35]. According to Table 2, the  $n$  value for the MWCNT-NH<sub>2</sub>/GA50% sample is higher than that of the other samples, indicating the formation of a consistent, protective layer on the metal surface.



**Figure 6.** Nyquist plots of (a) blank, (b) MWCNT-NH<sub>2</sub>, (c) MWCNT-NH<sub>2</sub>/25% GA, (d) MWCNT-NH<sub>2</sub>/50% GA, and (e) MWCNT-NH<sub>2</sub>/70% GA during 72 h exposure in 3.5 % NaCl solution.



**Figure 7.** Bode plots of (a) blank, (b) MWCNT-NH<sub>2</sub>, (c) MWCNT-NH<sub>2</sub>/25% GA, (d) MWCNT-NH<sub>2</sub>/50% GA, and (e) MWCNT-NH<sub>2</sub>/75% GA during 72 h exposure in 3.5 % NaCl solution.



**Figure 8.** EEC used for EIS data fitting; (a) two-time constant and (b) one-time constant models.

**Table 2.** Fitting parameters for EIS measurements of the samples following 48 h of immersion in a 3.5 % sodium chloride solution.

Sample	time (h)	$R_f^1$ ( $\Omega \cdot \text{cm}^2$ )	$CPE_f Y_0^2$ ( $\mu\Omega^{-1} \cdot \text{cm}^{-2} \cdot \text{s}^n$ )	$n_f^3$	$R_{ct}^1$ ( $\Omega \cdot \text{cm}^2$ )	$CPE_{dl} Y_0^2$ ( $\mu\Omega^{-1} \cdot \text{cm}^{-2} \cdot \text{s}^n$ )	$n_{dl}^3$	$R_t$ ( $\Omega \cdot \text{cm}^2$ )
Blank	2	-	-	-	1915	126	0.73	1915
	4	-	-	-	1780	495	0.80	1780
	6	-	-	-	1603	425	0.74	1603
	24	-	-	-	1365	137	0.79	1365
	48	-	-	-	1134	177	0.74	1134
	72	-	-	-	1544	383	0.75	1544
MWCNT-NH <sub>2</sub>	2	867	256	0.85	589	74	0.87	1456
	4	1009	123	0.86	607	97	0.84	1616
	6	1601	109	0.82	574	104	0.80	2175
	24	1615	25	0.78	1111	41	0.77	2726
	48	1443	194	0.89	1131	156	0.71	2574
	72	435	173	0.80	359	87	0.80	794
MWCNT-NH <sub>2</sub> /GA 25%	2	1172	256	0.85	532	108	0.87	1708
	4	1014	123	0.86	502	95	0.84	1516
	6	1601	109	0.82	905	167	0.80	2506
	24	1193	157	0.78	1367	124	0.77	4679
	48	1567	194	0.99	1131	89	0.81	2698
	72	457	172	0.84	229	112	0.80	686
MWCNT-NH <sub>2</sub> /GA 50%	2	647	145	0.99	870	288	0.83	1517
	4	1935	276	0.85	985	373	0.89	2920
	6	2418	225	0.92	1080	436	0.98	3498
	24	3668	453	0.98	1121	127	0.93	4789
	48	4076	154	0.91	1062	151	0.95	5138
	72	2045	198	0.83	949	153	0.85	2994
MWCNT-NH <sub>2</sub> /GA 75%	2	2489	225	0.74	876	76	0.76	3365
	4	1456	129	0.76	964	98	0.85	2420
	6	1683	186	0.87	688	102	0.86	2371

	24	1209	134	0.91	1101	115	0.80	1789
	48	1006	98	0.71	546	78	0.78	1647
	72	436	101	0.75	198	54	0.76	634

1 The standard deviation range for R is in the range of 1.2-5.8%.

2 The standard deviation for  $Y_0$  is in the range of 3.7-10.4%.

3 The standard deviation range for n is in the range of 0.5-3.1%.

### 3.2.2. Polarization

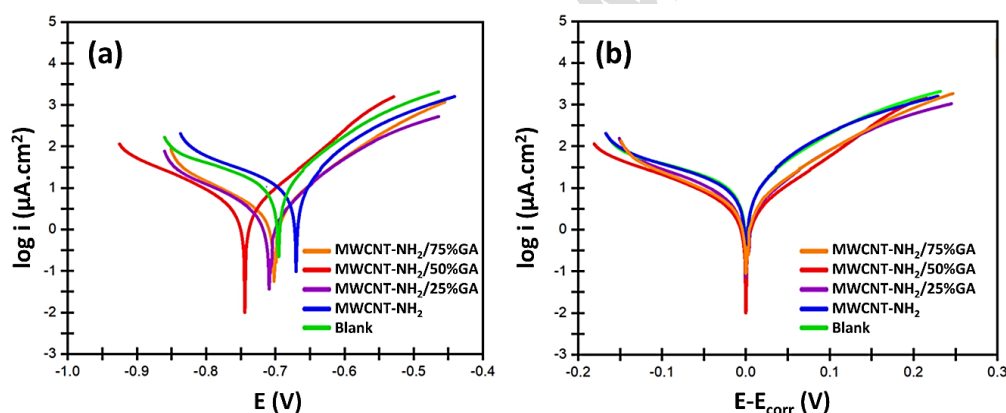
To examine the inhibition mechanism and quantify the corrosion rate, potentiodynamic polarization tests were conducted. Figure 9a presents the polarization curves obtained for metal samples immersed in a 3.5 wt% NaCl solution containing MWCNT-NH<sub>2</sub>/GA after 72 hours of exposure. Corrosion parameters were extracted using the Tafel extrapolation method and are summarized in Table 3. These include corrosion potential ( $E_{\text{corr}}$ ), corrosion current density ( $i_{\text{corr}}$ ), anodic Tafel slope ( $\beta_a$ ), cathodic Tafel slope ( $\beta_c$ ), polarization resistance ( $R_p$ ), and corrosion rate (CR). To facilitate clearer comparison of the corrosion mechanisms, the graphs were adjusted to  $E_{\text{corr}} = 0$  (Figure 9b). As can be observed, the slope of the graph is reduced in both the cathodic and anodic regions. In this way, the cations released from the particles move towards the cathodic part of the surface and, by forming an oxide-hydroxide layer, limit the cathodic reaction. Furthermore, the released gallate ions have one non-bonded electron pair and can act as an organic inhibitor. Consequently, it becomes adsorbed onto the anodic regions of the surface and regulates the metal oxidation process.

Notably, the cathodic Tafel slope exhibited a more pronounced decrease, particularly for the MWCNT-NH<sub>2</sub>/GA25% and MWCNT-NH<sub>2</sub>/GA50% samples. The  $E_{\text{corr}}$  values also shifted negatively with increasing MWCNT-NH<sub>2</sub>/GA content, suggesting that both

anodic and cathodic reactions were influenced, with cathodic inhibition dominant.

**Table 3.** Fitting parameters for EIS measurements of the mild steel samples following 72 h immersion in 3.5 % NaCl solution.

Sample	$E_{corr}$ (V)	$i_{corr}$ ( $\mu\text{A}/\text{cm}^2$ )	$\beta_a$ (V/dec)	$-\beta_c$ (V/dec)
bare	$-0.671 \pm 0.01$	$4.15 \pm 0.3$	$0.066 \pm 0.005$	$0.093 \pm 0.005$
CNT-NH <sub>2</sub>	$-0.694 \pm 0.01$	$2.59 \pm 0.03$	$0.06 \pm 0.005$	$0.09 \pm 0.01$
CNT-NH <sub>2</sub> /GA25%	$-0.706 \pm 0.01$	$2.28 \pm 0.2$	$0.043 \pm 0.004$	$0.065 \pm 0.01$
CNT-NH <sub>2</sub> /GA50%	$-0.741 \pm 0.01$	$2.2 \pm 0.2$	$0.026 \pm 0.004$	$0.049 \pm 0.02$
CNT-NH <sub>2</sub> /GA75%	$-0.702 \pm 0.01$	$2.96 \pm 0.3$	$0.05 \pm 0.003$	$0.067 \pm 0.02$



**Figure 9.** (a) Polarization, and (b) shifted polarization curves to  $E = 0$  of steel samples immersed in 3.5% salt solutions for 72 h in 3.5 % NaCl solution.

### 3.3. Coating-phase investigation

#### 3.3.1. Scratched coatings

The corrosion behavior of the Scratched steel electrodes protected by EP, EP-NH<sub>2</sub>-MWCNT, EP-NH<sub>2</sub>-MWCNT/GA25%, EP-MWCNT-NH<sub>2</sub>/GA50%, and EP-MWCNT-NH<sub>2</sub>/GA75% coatings was evaluated by EIS measurements in saline solution. The

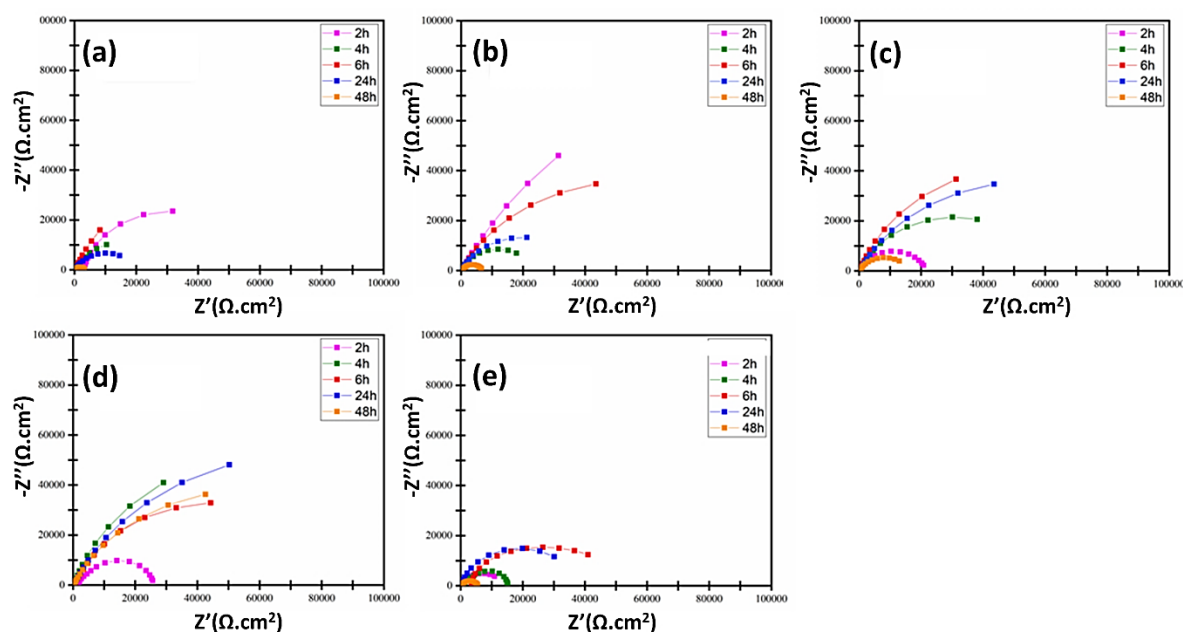


Nyquist and Bode plots are illustrated in Figures 10 and 11, respectively. The arc diameter declines in the EP and EP-MWCNT-NH<sub>2</sub> plots as immersion time increases, indicating a hastening of the corrosion process. The highest arc diameter observed in the EP and EP-MWCNT-NH<sub>2</sub> samples was approximately 50 kΩ.cm<sup>2</sup> and 65 kΩ.cm<sup>2</sup> after two hours of immersion, whereas the EP-MWCNT-NH<sub>2</sub>/GA exhibited arc diameters of around 20 kΩ.cm<sup>2</sup> during the same duration. Nevertheless, the highest arc diameter in the EP-MWCNT-NH<sub>2</sub>/GA25% samples rose to about 90 kΩ.cm<sup>2</sup>, 120 kΩ.cm<sup>2</sup>, and 255 kΩ.cm<sup>2</sup> in the EP-MWCNT-NH<sub>2</sub>/GA25%, EP-MWCNT-NH<sub>2</sub>/50%GA, and EP-MWCNT-NH<sub>2</sub>/75%GA samples, respectively. This increase in arc diameter was observed after 24 hours of immersion for the EP-MWCNT-NH<sub>2</sub>/50%GA and EP-MWCNT-NH<sub>2</sub>/25%GA samples, and after 6 hours for the EP-MWCNT-NH<sub>2</sub>/75%GA sample, highlighting the effective protective properties of these nanomaterials within a polymer coating.

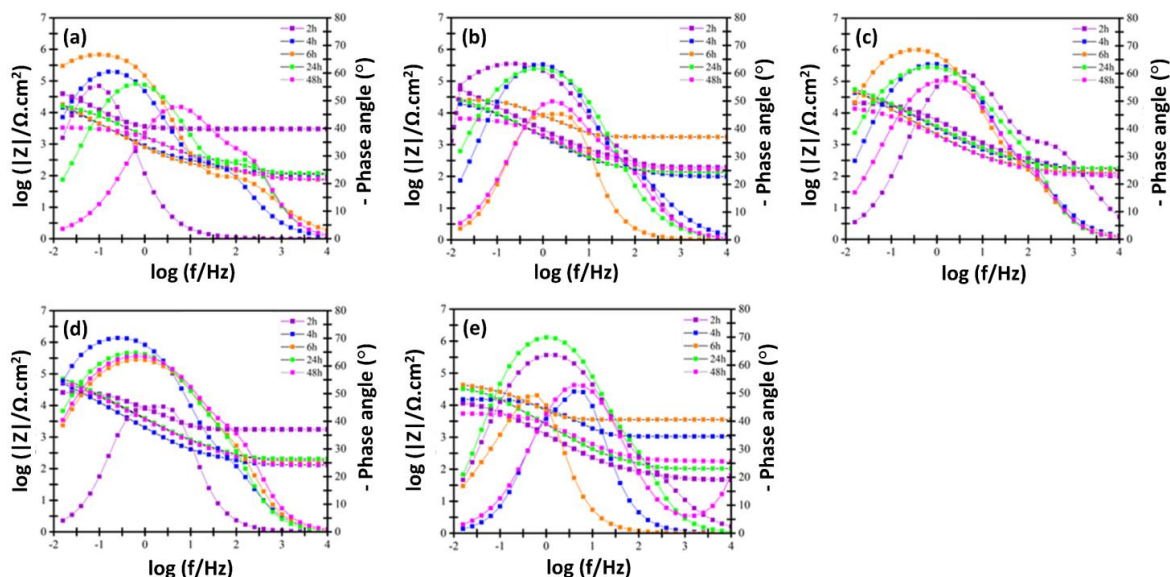
The significant increase in the resistance of EP-MWCNT-NH<sub>2</sub>/25%GA coatings compared to inhibitor-free polymer coatings demonstrates the presence of effective active protection. If a scratch or defect arises in coatings that incorporate MWCNT-NH<sub>2</sub>/GA nanocomposites, GA inhibitor ions are liberated from the MWCNT-NH<sub>2</sub> particles and subsequently enter the electrolyte. Gallate ions are released partially, forming a protective layer in the scratched area following prolonged exposure to the saline environment, thereby preventing the electrolyte from directly contacting the metal substrate. The outcome is the management of water infiltration and the minimization of corrosion-related damage, ultimately enhancing the overall effectiveness of the impaired coating [20, 21, 32]. The  $\log|Z|_{10 \text{ mHz}}$  value serves as an appropriate metric for assessing film

development in the scratched area. It exhibited a decline in the EP and EP-MWCNT-NH<sub>2</sub> samples throughout the immersion period, ultimately dropping below 0.4 k $\Omega$ .cm<sup>2</sup> after 24 hours. Conversely, in the epoxy samples containing EP-MWCNT-NH<sub>2</sub>/50%GA, this value rose to approximately 4.8 k $\Omega$ .cm<sup>2</sup> after 24 hours of immersion and remained above 0.4 k $\Omega$ .cm<sup>2</sup> even after 48 hours.

The log|Z|<sub>10 mHz</sub> values for the EP-MWCNT-NH<sub>2</sub>/25%GA coatings are higher than those for the EP and EP-MWCNT-NH<sub>2</sub> samples at each of the times when the test was performed. The EIS test fully confirms that the MWCNT-NH<sub>2</sub>/GA nanocomposites form a surface film and provide active protection for the polymer coating. The data obtained from scratched samples are in agreement with the findings and analysis of the corrosion protection evaluation tests in solution (Section 3.2).



**Figure 10.** Nyquist plots of (a) EP, (b)EP-MWCNT-NH<sub>2</sub>, (c) EP-MWCNT-NH<sub>2</sub>/25% GA, (d) EP-MWCNT-NH<sub>2</sub>/50% GA, and (e) EP-MWCNT-NH<sub>2</sub>/75% GA scratched coatings during 48 h exposure to 3.5 % NaCl solution.



**Figure 11.** Bode plots of the (a) EP, (b) EP-MWCNT-NH<sub>2</sub>, (c) EP-MWCNT-NH<sub>2</sub>/25% GA, (d) EP-MWCNT-NH<sub>2</sub>/50% GA, and (e) EP-MWCNT-NH<sub>2</sub>/75% GA scratched coatings during 48 h exposure in 3.5 % NaCl solution.

### 3.3.2. Salt spray and surface analysis

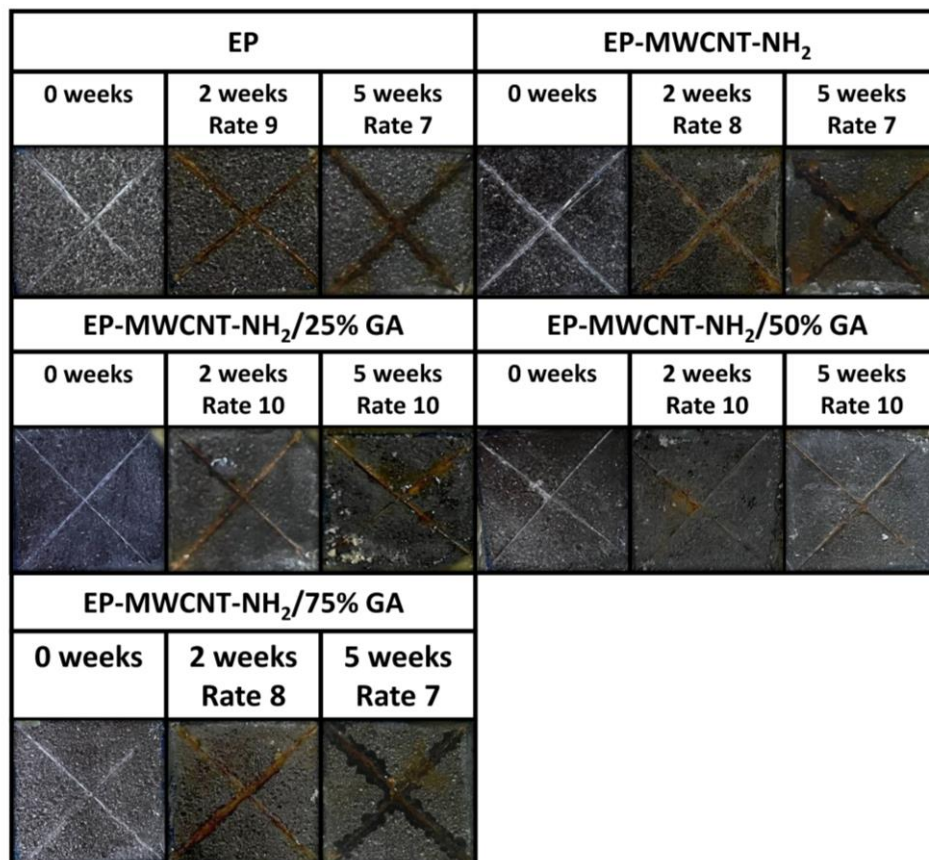
To evaluate the active protection effect of the samples in both short-term and long-term applications, the scratched coatings were placed in a salt spray chamber. The failure rating at scratch was assessed according to procedure A of ASTM D 1654. The images of the damaged samples under salt spray conditions and their failure ratings at different times are shown in Figure 12. The EP sample had more corrosion products around the scratch. This indicates significant diffusion of corrosive ions into the coating and deeper corrosion penetration, leading to a notable detachment of the film from the substrate around the scratch.

The EP-MWCNT-NH<sub>2</sub> sample demonstrated the formation of water droplets beneath the coating during the first week. The presence of corrosion products and iron rust in the scratched region has indeed led to water infiltration beneath the coating, causing it to

detach from the metal surface. After 2 and 5 weeks of salt-spray exposure, numerous regions have been observed where the coating has become detached from the metal, indicating reduced adhesion at the interface between the coating and the metal.

EP-MWCNT-NH<sub>2</sub>/GA25% and EP-MWCNT-NH<sub>2</sub>/GA50% demonstrated superior performance compared to EP-MWCNT-NH<sub>2</sub>/GA75% sample during prolonged exposure.

The EP-MWCNT-NH<sub>2</sub>/GA75% sample exhibited severe rusting after 2 weeks, and after 5 weeks, the coating surrounding the scratches was nearly detached, suggesting that GA molecules provided inefficient protection. However, at percentages below this level, the coating demonstrated satisfactory corrosion resistance. It was noted that EP-MWCNT-NH<sub>2</sub>/GA50% had the best performance and produced fewer corrosion products, consistent with EIS data confirming that the MWCNT-NH<sub>2</sub>/50%GA nanocomposites can provide effective active protection for the epoxy coating. There was no significant occurrence of rust or delamination even after 5 weeks.

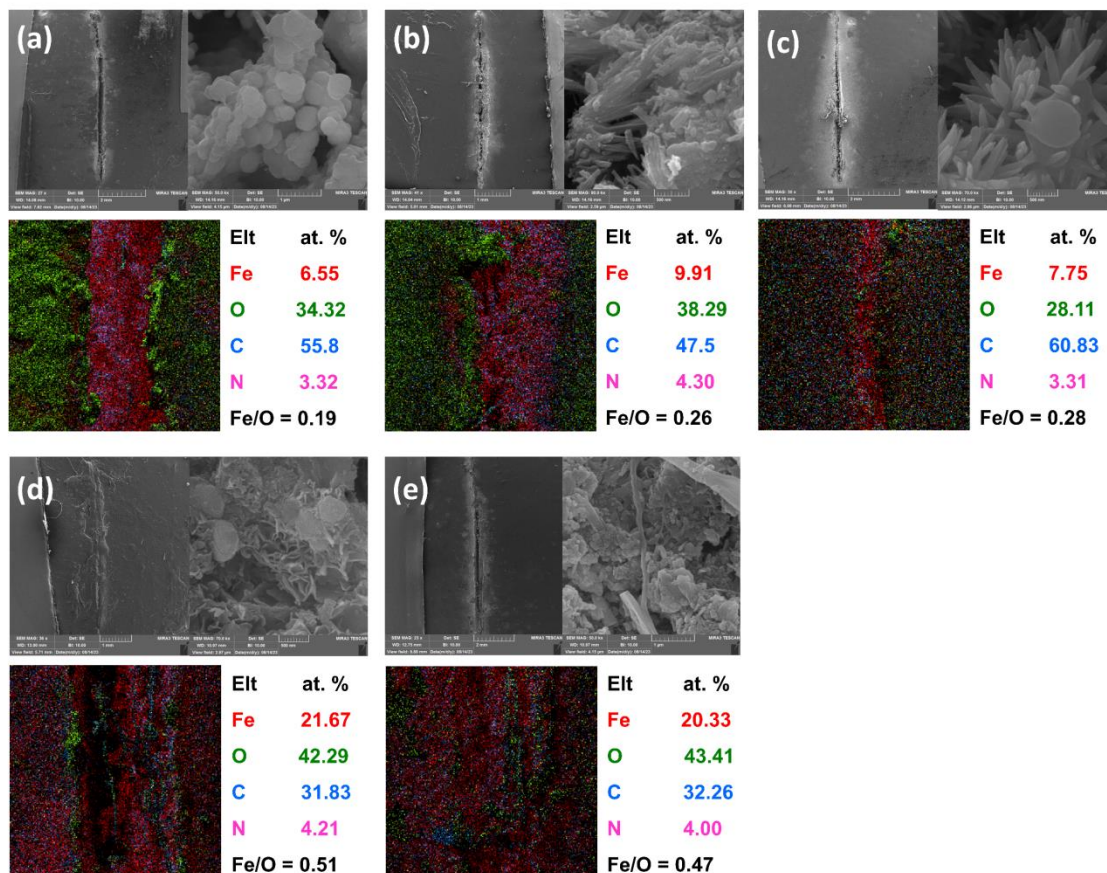


**Figure 12.** Optical images of Salt spray tests during 5 weeks for EP and EP-MWCNT-NH<sub>2</sub>-GA x% (x=0, 25, 50, and 75) and their rating according to procedure A of ASTM D 1654 standard.

The FE-SEM microscopic images displayed in Figure 13 illustrate the surface of the samples within the scratched line under the salt spray test. The morphology of the EP and EP-MWCNT-NH<sub>2</sub> sample is entirely nonuniform, porous, and covered with corrosion products. In GA-containing samples, a uniform inhibitory film is observed, indicating that GA interacts with the surface through physical and chemical interactions, forming a GA-based inhibitory film. The images reveal that the inhibitory film in the EP-MWCNT-NH<sub>2</sub>/GA50% sample is adequately smooth, and the corrosion products on the substrate are not discernible, indicating its effective anticorrosion performance. By incorporating

the MWCNT-NH<sub>2</sub>/GA nanocomposite into the epoxy, the layer smoothness has slightly decreased; however, the inhibitory layer density remains acceptable, suggesting enhanced anticorrosion performance. The atomic ratio of Fe to O can reflect the relative amounts of metallic iron in relation to oxygen-rich corrosion products. Consequently, an increased Fe/O ratio suggests greater exposure of metallic iron and fewer corrosion products. EDS analysis shown in Figure 13 aligns with the morphological studies and electrochemical analyses, demonstrating that the Fe/O ratio was approximately 0.19 in the EP coating and rose to nearly 0.51 in the EP-MWCNT-NH<sub>2</sub>/GA50% coating, suggesting a decrease in the generation of corrosion products.

The protection facilitated by GA molecules relies on both physical and chemical interactions. When GA is dissolved in the medium, it can undergo protonation. The presence of free H<sup>+</sup> ions in solution allows them to interact with neutral GA, thereby protonating it. Subsequently, the charged gallate ions are inclined to interact with pre-adsorbed chlorides via electrostatic interactions, leading to physical adsorption. Furthermore, gallate ions can donate electrons from the C=O functional groups to the unfilled orbitals of Fe cations, leading to chemisorption via covalent bonding.



**Figure 13.** FESEM images and EDS mapping results of (a) EP, and (b-e) EP-MWCNT-NH<sub>2</sub>/GA x% (x=0, 25, 50, and 75) (with an artificial defect) after salt spray test exposure.

### 3.3.3. Pull-off

The adhesion strength of the samples was evaluated under both dry and wet conditions to examine the effect of MWCNT-NH<sub>2</sub>/GA on the adhesion of epoxy coatings to ST1 steel using a pull-off test. Before measuring wet adhesion, the samples were subjected to a salt spray chamber for 1 week. The test results, along with images of the samples post-measurement, are presented in Figure 14. The adhesion loss for all samples was determined using Eq. 1.

$$Adhesion\ loss = \frac{D-W}{D} \times 100 \quad (1)$$



In this equation, D and W are the adhesion strength values measured in dry and wet conditions, respectively. The adhesion loss values for Ep, Ep-MWCNT-NH<sub>2</sub>, Ep-MWCNT-NH<sub>2</sub>/GA25%, Ep-MWCNT-NH<sub>2</sub>/GA50% and Ep-MWCNT-NH<sub>2</sub>/GA75% were 58%, 53%, 16%, 6% and 21%, respectively. A considerable loss of adhesion was observed for the EP coating, which exhibited lower values in both dry and wet conditions than those of other samples. Adding MWCNT-NH<sub>2</sub>/GA to epoxy coatings reduced the rate of adhesion loss. MWCNT-NH<sub>2</sub>/GA improves the adhesion of the EP coating, especially in wet conditions, and provides a barrier effect.

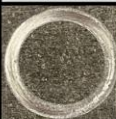
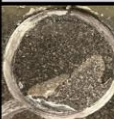
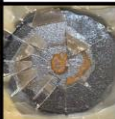
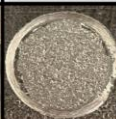
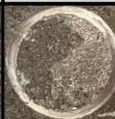
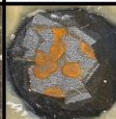


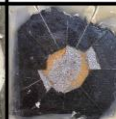


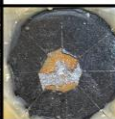
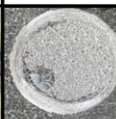

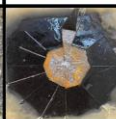
Adhesion loss can serve as an indirect indicator of a coating's hydrolytic stability [36]. Wet pull-off strength reflects the practical effect of hydrolytic degradation on coating adhesion. Thus, epoxy coatings with better hydrolytic stability tend to demonstrate higher retained pull-off strength after water exposure. Therefore, it can be inferred that among the different samples, Ep-MWCNT-NH<sub>2</sub>/GA50%, which showed an adhesion loss of 8%, had the best hydrolytic stability.

GA is capable of effectively grafting onto metallic surfaces by forming hydrogen bonds with the oxide layer on the surface, as well as by donating  $\pi$ -electrons from the benzene and C=O groups of GA to occupy the empty Fe orbitals [5, 21, 22]. It can function as a coupling agent or an interfacial modifier [14, 15]. Its interaction with metal oxides present on the steel surface leads to the formation of complexes that enhance surface roughness, potentially facilitating improved mechanical interlocking [16].

The surface modification of MWCNT-NH<sub>2</sub> by GA appears to enhance polar-polar interactions, such as hydrogen bonding, between the epoxy coating and the metal substrate. This improvement addresses the incompatibility between MWCNTs-NH<sub>2</sub> and



EP, reducing agglomeration and improving the uniform dispersion of MWCNT-NH<sub>2</sub>/GA within the polymeric matrix, thereby resulting in a higher adhesion value under dry conditions. Furthermore, the hydroxyl groups in GA can enhance the polar-polar interactions between the coating and the epoxy's hydroxyl groups. It is also observed that the trends in adhesion values closely match those in the release rate of gallate inhibitor ions. Under wet conditions, the OH<sup>-</sup> anions released from MWCNT-NH<sub>2</sub>/GA can interact with surface cations to form a film that possesses barrier properties against water and corrosive agents [20, 21]. Additionally, managing the increase in pH in cathodic regions helps prevent corrosion reactions, significantly reducing the rate of corrosion products formed at the interface between the coating and substrate, thereby preventing the coating from separating from the surface.

EP			EP-MWCNT-NH <sub>2</sub>			EP-MWCNT-NH <sub>2</sub> /25% GA		
Dry pull-off	Wet pull-off	Cathodic disbondment	Dry pull-off	Wet pull-off	Cathodic disbondment	Dry pull-off	Wet pull-off	Cathodic disbondment
								
4.05 MPa	1.69 MPa	CDR= 13.42 mm	5.99 MPa	2.82 MPa	CDR= 11.96 mm	2.80 MPa	2.32 MPa	CDR= 6.95 mm
EP-MWCNT-NH <sub>2</sub> /50% GA			EP-MWCNT-NH <sub>2</sub> /75% GA					
Dry pull-off	Wet pull-off	Cathodic disbondment	Dry pull-off	Wet pull-off	Cathodic disbondment			
								
4.52 MPa	4.28 MPa	CDR= 6.27 mm	2.75 MPa	1.72 MPa	CDR= 7.83 mm			

**Figure 14.** Visual performance, pull-off strength, and the average disbondment radius (CDR) of EP and EP-MWCNT-NH<sub>2</sub>-GA x% (x=0, 25, 50, and 75) samples following pull-off and the cathodic delamination examination.

### 3.3.4. Cathodic delamination

The adhesion of the coatings was examined under cathodic polarization conditions. The findings and images depicting the coatings that detached from the surface following the test are presented in Figure 14. After 24 hours, reduced coating detachment from the surface is observed in the EP-MWCNT-NH<sub>2</sub>/GA50% samples compared to other samples. Furthermore, the detached coating in the Ep-MWCNT-NH<sub>2</sub>/GA50% sample exhibited the smallest average diameter among the other samples, consistent with other results and demonstrating the superior performance of MWCNT-NH<sub>2</sub>/GA50% in epoxy coatings. The OH<sup>-</sup> ions generated in the cathodic areas and beneath the epoxy coatings are the main contributors to increased pH in these areas, leading to diminished adhesion and detachment of the epoxy coating from the surface. Gallate ions can directly interact with sodium ions, thereby inhibiting the completion of the hydrolysis process. Given its negative charge and anionic nature, gallate ions interact with sodium ions with high probability, and by regulating their interaction with sodium hydroxide ions, pH fluctuations are prevented, allowing for significant control over the hydrolysis process. Therefore, EP coatings containing MWCNT-NH<sub>2</sub>/GA could better withstand the cathodic delamination.

Moreover, the presence of GA molecules with abundant hydroxyl and carboxyl groups enhances adhesion via hydrogen bonding with the surface oxide layer. Additionally, the empty orbitals of Fe can be occupied through the donation of  $\pi$ -electrons from benzene and the C=O groups of GAs, leading to increased adhesion at the interface [5, 21, 22]. Therefore, GA-loaded MWCNT-NH<sub>2</sub> incorporation can improve the adhesion bond's resistance.

GA is a polyphenolic compound with antioxidant activity that functions as a free radical

scavenger that inhibits oxidation by directly entering the autoxidation chain by neutralizing the free radicals, which is controlled by the donation of hydrogen atoms from the phenolic OH<sup>-</sup> ions generated in the cathodic regions and beneath the epoxy coatings. The free radical scavenger species is essentially consumed in this process. The resulting antioxidant radical (phenoxyl radical) is resonance-stabilized and much less reactive, preventing the propagation of radical chain reactions. However, the phenoxyl radical can still recombine with a second free radical. Therefore, GA recombines with the intermediate radicals formed during hydroxyl group formation, thereby inhibiting their rapid generation in the cathodic areas. This, in turn, serves as a restraint on the extensive cathodic separation phenomenon [17, 37]. These findings illustrate the remarkable effectiveness of the MWCNT-NH<sub>2</sub>/GA nanocomposite in minimizing cathodic delamination.

### 3.3.5. Dynamic Mechanical Thermal Analysis

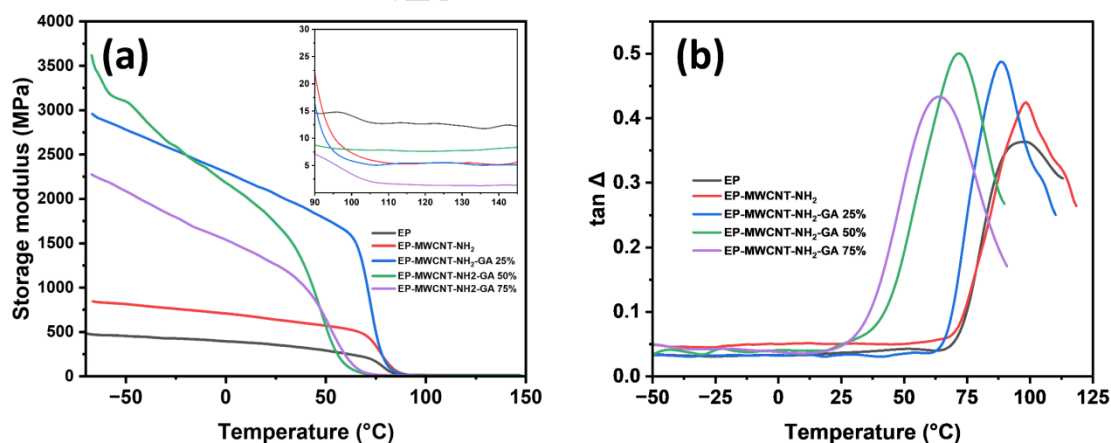
The variations in loss tangent (tan Δ) and storage modulus for various samples as a function of temperature are illustrated in Figure 15. Furthermore, the derived thermomechanical parameters are presented in Table 4. The crosslinking density (ν<sub>e</sub>) was calculated using Eq. 2 [38].

$$\nu_e = \frac{E'_R}{3RT} \quad (2)$$

where  $E'_R$  Designates the storage modulus in the rubbery region; T and R denote the absolute temperature (K) and the ideal gas constant, respectively.

The incorporation of GA into the structure enhances the storage modulus, thereby improving the sample's elastic characteristics (Figure 15a). Conversely, as depicted in

Figure 15b and Table 4, an increase in the GA-loading within the structure results in a reduction in the glass transition temperature ( $T_g$ ). As anticipated, a greater proportion of GA is associated with a more pronounced decrease in  $T_g$ . GA interferes with the curing of epoxy. Phenolic OH and carboxyl groups of GA can form bonds with amine groups of polyamide hardener, which can slow down diffusion or reduce amine availability for curing epoxy [39]. This will result in lower  $v_e$  and  $T_g$  values for EP-MWCNT-NH<sub>2</sub>/GA coatings. Decreasing the degree of crosslinking signifies fewer covalent bonds connecting the epoxy polymer chains, thereby providing epoxy network segments with greater flexibility and mobility, which allows the material to absorb more energy when under stress (i.e., increased toughness) [40]. Interestingly, the addition of MWCNT-NH<sub>2</sub> did not significantly alter the  $T_g$  or storage modulus. However, surface modification with GA improved the sample's toughness.



**Figure 15.** (a) Variation of the loss modulus versus temperature for EP and EP-MWCNT-NH<sub>2</sub>/GA x% (x=0, 25, 50, and 75), and (b) Variation of the tanΔ versus temperature.

**Table 4.** The derived thermomechanical parameters from DMTA analysis.

Sample	$E'_g$	$E'_R$	$\tan\Delta$ peak height	$T_g$ (°C)	$v_e$ (mol/cm <sup>3</sup> )
EP	217.02	12.88	0.36	96	0.001403
EP-MWCNT-NH <sub>2</sub>	499.6	5.81	0.42	98.3	0.000616
EP-MWCNT-NH <sub>2</sub> /GA 25%	1624.9	5.81	0.48	88.3	0.000625
EP-MWCNT-NH <sub>2</sub> /GA 50%	1555.4	8.21	0.5	71.7	0.000902
EP-MWCNT-NH <sub>2</sub> /GA 75%	118.7	2.04	0.43	64	0.000216

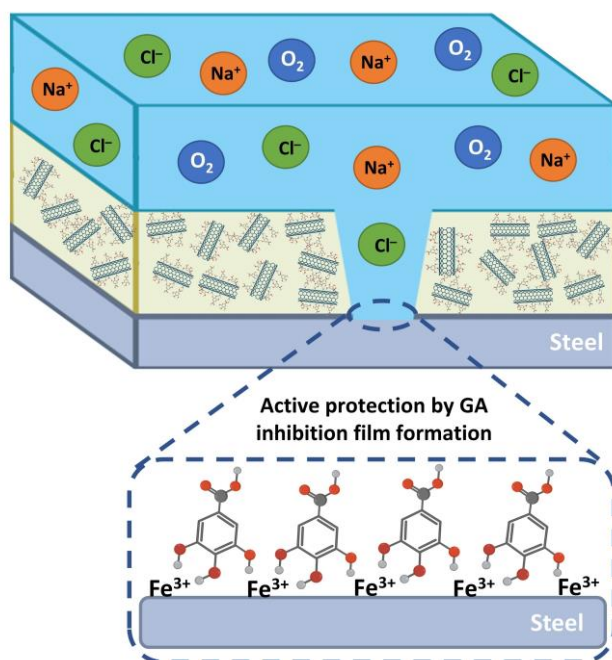
### 3.4. Corrosion inhibition mechanism

Figure 16 provides a schematic representation of the anticorrosion and self-healing mechanisms associated with MWCNT-NH<sub>2</sub>/GA incorporated into epoxy coatings. By surface-modifying MWCNT-NH<sub>2</sub> with GA, both barrier and active protection can be simultaneously provided to the EP coating. MWCNTs-NH<sub>2</sub> exhibit barrier properties attributed to their high specific surface area and three-dimensional structure. The cylindrical configuration of MWCNTs is crucial and significantly influences the pathway the electrolyte must traverse to reach the metal/coating interface. Nevertheless, their hydrophobic nature impedes effective dispersion in organic media, resulting in aggregation. Consequently, they do not provide a robust barrier against corrosive agents. However, following modification with GA, the barrier properties showed considerable enhancement due to improved particle dispersion in organic media and reduced aggregation, with this effect becoming more evident in the corrosion test results [28, 41]. Moreover, GA exhibits partial solubility in water, allowing it to release gallate ions into the solution. In the event of a scratch on the epoxy coating, the MWCNT-NH<sub>2</sub>/GA interacts with the electrolyte, releasing gallate anions in the affected area and rendering

the self-healing properties. At the microscale, gallate anions adhere to the metal surface. The adsorption process is promoted by the functional groups present in gallic acid, specifically the hydroxyl and carboxyl groups. GA can interact with steel both physically and chemically [20, 21, 42]. The vacant orbitals of Fe will be filled through the donation of  $\pi$ -electrons from benzene and the C=O groups of GAs, leading to chemical reactions that facilitate the adsorption of GAs. At the same time, the OH groups present on the GAs will anchor to the steel surface by interacting with the oxide layer via hydrogen bonding and chelation with surface Fe sites [43, 44].

Consequently, a thin protective layer is established on the metal surface, effectively controlling corrosion reactions. In contrast, if MWCNT-NH<sub>2</sub> is utilized alone in the coating, it fails to prevent metal degradation reactions. Among the samples containing varying percentages of inhibitor, the 50% GA sample exhibited superior corrosion resistance compared to the 25% GA sample. It can be concluded that these findings are more favorable due to the increased quantity of inhibitor. However, for the 75% GA sample, increasing the inhibitor amount does not necessarily improve coating properties, as this increase may interfere with film formation. When the corrosion inhibitor is added in excess, it can hinder the proper dispersion and adhesion of the coating material. This may lead to uneven coating, cracks, or inadequate adhesion to the substrate. Consequently, the coating's ability to provide effective corrosion protection is compromised. Coatings must possess specific mechanical properties, including hardness, flexibility, and impact resistance, to endure various conditions. Excessive addition of inhibitors can alter the molecular structure and interactions within the coating matrix. Consequently, this may lead to coatings that are overly soft, brittle, or deficient in the

flexibility required to endure mechanical stress.



**Figure 16.** Schematic representation of the anticorrosion mechanism of MWCNT-NH<sub>2</sub>/GA nanocomposites in epoxy resin coating.

#### 4. Conclusions

Results demonstrate that surface modification of MWCNT-NH<sub>2</sub> with GA was successfully performed in three distinct ratios of GA (MWCNT-NH<sub>2</sub>/25% GA, MWCNT-NH<sub>2</sub>/50% GA, and MWCNT-NH<sub>2</sub>/75%GA). Electrochemical assessments conducted in solution demonstrated the development of an active protective effect using MWCNT-NH<sub>2</sub>/GA. The total corrosion resistance obtained in the electrochemical impedance test for the MWCNT-NH<sub>2</sub>/25%GA, MWCNT-NH<sub>2</sub>/50%GA, and MWCNT-NH<sub>2</sub>/75%GA after 24 hours of immersion was 37%, 58%, and 32% greater than that of the saline solution devoid of nanoparticles, respectively. Among them, MWCNT-NH<sub>2</sub>/50%GA released the most significant quantity of gallate ions into the electrolyte.

The electrochemical impedance test, along with the salt spray test on scratched EP coatings containing MWCNT-NH<sub>2</sub>/GA, further validated the formation of an active protection layer within the epoxy coating. All GA-containing MWCNT-NH<sub>2</sub> particles imparted a self-healing effect to the coating. The evaluation of the scratch site was performed using FESEM and EDS. The findings regarding cathodic separation and adhesion under both dry and wet conditions also indicated enhanced adhesion in coatings incorporating MWCNT-NH<sub>2</sub>/GA. The MWCNT-NH<sub>2</sub>/GA50% was the most effective in delivering active corrosion protection and enhancing adhesion, attributed to their superior release of gallate ions and favorable compatibility and dispersion within the EP coating. Consequently, the immobilization of GA on MWCNTs provides a highly effective, environmentally friendly method for enhancing the active corrosion protection capabilities of epoxy coatings.

## References

1. Koch G. 1 - Cost of corrosion. In: El-Sherik AMBTT in O and GCR and T, editor. Woodhead Publishing Series in Energy [Internet]. Boston: Woodhead Publishing; 2017. 330. <https://doi.org/10.1016/B978-0-08-101105-8.00001-2>.
2. Zhao Y, Yan S, He Y, Li Z, Li C, Li H. Synthesis of ultrathin  $\alpha$ -zirconium phosphate functionalized with polypyrrole for reinforcing the anticorrosive property of waterborne epoxy coating. *Colloids Surfaces A Physicochem Eng Asp*. 2022;635:128052. <https://doi.org/10.1016/j.colsurfa.2021.128052>.
3. Zhang T, Zhang Y, Chen C, Tian Y, Wang Y, Cao S, et al. Corrosion-resistant SiO<sub>2</sub>-graphene oxide/epoxy coating reinforced by effective electron beam curing. *Prog Org Coat*. 2023; 184:107855. <https://doi.org/10.1016/j.porgcoat.2023.107855>.
4. Sharma N, Sharma S, Sharma SK, Mahajan RL, Mehta R. Investigations on corrosion inhibition performance of self-healing nano-clay modified epoxy



- coatings. J Build Eng. 2023; 70:106368.  
<https://doi.org/10.1016/j.jobe.2023.106368>.
5. Liu R, Wang X, Wang J, Lin Z, Chen L, Li Z, et al. Gallic acid-modified montmorillonite reinforced acrylic latex composite coatings: enhanced mechanical and anticorrosion performances via barrier and interface passivation. Prog Org Coat. 2026; 210:109649. <https://doi.org/10.1016/j.porgcoat.2025.109649>.
6. Liu X, Chen Q, Fan Z, Liu C, Wu H. Enhanced anticorrosion of waterborne epoxy coating with MWCNTs-CeO<sub>2</sub>@PDA incorporation. Ind Eng Chem Res. 2025; 64(39):19064-74. <https://doi.org/10.1021/acs.iecr.5c02042>
7. Hughes KJ, Iyer KA, Bird RE, Ivanov J, Banerjee S, Georges G, et al. Review of carbon nanotube research and development: materials and emerging applications. ACS Appl Nano Mater. 2024; 7(16):18695-713.  
<https://doi.org/10.1021/acsanm.4c02721>
8. Ijaz H, Mahmood A, Abdel-Daim MM, Sarfraz RM, Zaman M, Zafar N, et al. Review on carbon nanotubes (CNTs) and their chemical and physical characteristics, with particular emphasis on potential applications in biomedicine. Inorg Chem Commun. 2023; 155:111020.  
<https://doi.org/10.1016/j.inoche.2023.111020>.
9. Han Z, Fina A. Thermal conductivity of carbon nanotubes and their polymer nanocomposites: A review. Prog Polym Sci. 2011;36(7):914-44.  
<https://doi.org/10.1016/j.progpolymsci.2010.11.004>.
10. Ma PC, Mo SY, Tang BZ, Kim JK. Dispersion, interfacial interaction and re-agglomeration of functionalized carbon nanotubes in epoxy composites. Carbon N Y. 2010; 48(6):1824–34. <https://doi.org/10.1016/j.carbon.2010.01.028>.
11. Zhang Q, Wu J, Gao L, Liu T, Zhong W, Sui G, et al. Dispersion stability of functionalized MWCNT in the epoxy–amine system and its effects on mechanical and interfacial properties of carbon fiber composites. Mater Des. 2016;94:392-402.  
<https://doi.org/10.1016/j.matdes.2016.01.062>.
12. Jeon H, Park J, Shon M. Corrosion protection by epoxy coating containing multi-walled carbon nanotubes. J Ind Eng Chem. 2013; 19(3):849-53.  
<https://doi.org/https://doi.org/10.1016/j.jiec.2012.10.030>.

13. Nayak SR, Mohana KNS, Hegde MB, Rajitha K, Madhusudhana AM, Naik SR. Functionalized multi-walled carbon nanotube/polyindole incorporated epoxy: An effective anti-corrosion coating material for mild steel. *J Alloys Compd.* 2021; 856:158057. <https://doi.org/10.1016/j.jallcom.2020.158057>.
14. Ferraris S, Cazzola M, Ubertalli G, Prenesti E, Spriano S. Grafting of gallic acid to metallic surfaces. *Appl Surf Sci.* 2020; 511:145615. <https://doi.org/10.1016/j.apsusc.2020.145615>.
15. Wang Z, Zhu X, Yu Q, Feng X, Zhao Y, Chen L. Gallic acid—polyethyleneimine modified UHMWPE fibers with epoxy resin for investigating interfacial properties. *J Polym Res.* 2024; 31(4):116. <https://doi.org/10.1007/s10965-024-03960-2>
16. Zaragoza N, Widder S, Huynh H, Zamani M, Furst AL. Electrocatalytic Properties of Electrochemically-Polymerized Metal-Phenolic Networks. *Chem Electro Chem.* 2024; 11(10):e202400093. <https://doi.org/10.1002/celec.202400093>
17. Sesia R, Spriano S, Sangermano M, Ferraris S. Natural polyphenols and the corrosion protection of steel: recent advances and future perspectives for green and promising strategies. *Metals.* 2023; 13(6): 1070. <https://doi.org/10.3390/met13061070>.
18. Sileika TS, Barrett DG, Zhang R, Lau KHA, Messersmith PB. Colorless Multifunctional Coatings Inspired by Polyphenols Found in Tea, Chocolate, and Wine. *Angew Chemie Int Ed.* 2013; 52(41):10766-70. <https://doi.org/10.1002/anie.201304922>
19. Shi H, Pan K, Dai M, Wei W, Liu X, Li X. A Gallic Acid-Doped Polypyrrole Coating with Anticorrosion and Antibacterial Properties on Magnesium Alloy. *ACS Appl Bio Mater.* 2022; 5(9):4244-55. <https://doi.org/10.1021/acsabm.2c00453>
20. Akbari YHA, Rostami M, Sari MG, Ramezanzadeh B. Gallic acid-infused LDH nano-containers: A durable protection against mild steel corrosion in simulated seawater. *J Mol Struct.* 2024; 1309:138034. <https://doi.org/10.1016/j.molstruc.2024.138034>.
21. Akbari YHA, Rostami M, Sari MG, Ramezanzadeh B. Evaluation of MgAl LDH

- incorporated Gallic acid anti-corrosion impact on mild steel in tempered 3.5% NaCl solutions: Integrated electrochemical and morphological studies. *J Ind Eng Chem.* 2023; 127:365-77. <https://doi.org/10.1016/j.jiec.2023.07.021>.
22. Zhao C, Wang C, Li Y, Yuan W, Huang Y, Cheng D, et al. Developing anticorrosion epoxy composite coating based on PEG-gallic acid complex functionalized two-dimensional zeolitic imidazolate framework nanosheets. *Prog Org Coat.* 2025;209:109618. <https://doi.org/10.1016/j.porgcoat.2025.109618>.
23. Luzi F, Pannucci E, Santi L, Kenny JM, Torre L, Bernini R, et al. Gallic acid and quercetin as intelligent and active ingredients in poly(vinyl alcohol) films for food packaging. *Polymers.* 2019; 11(12): 1999. <https://doi.org/10.3390/polym11121999>.
24. Karaca MA, Kamali AR, Kamali BE, Temiz B, Özben F, Ege D, et al. Gallic acid loaded alginate-gelatin beads for potential bone tissue engineering applications. *biopolymers.* 2025; 116(4):e70033. <https://doi.org/10.1002/bip.70033>
25. Hirun N, Dokmaisrijan S, Tantishaiyakul V. Experimental FTIR and theoretical studies of gallic acid–acetonitrile clusters. *Spectrochim Acta Part A Mol Biomol Spectrosc.* 2012; 86:93-100. <https://doi.org/10.1016/j.saa.2011.10.009>.
26. Jimeno A, Goyanes S, Eceiza A, Kortaberria G, Mondragon I, Corcuera MA. Effects of amine molecular structure on carbon nanotubes functionalization. *J Nanosci Nanotechnol.* 2009; 9(10):6222-7. <https://doi.org/10.1166/jnn.2009.1562>.
27. Zanganeh S, Khodadadei F, Tafti SR, Abdolahad M. Folic acid functionalized vertically aligned carbon nanotube (FA-VACNT) electrodes for cancer sensing applications. *J Mater Sci Technol.* 2016; 32(7):617-25. <https://doi.org/10.1016/j.jmst.2016.05.001>.
28. Rajavel K, Gomathi R, Manian S, Rajendra Kumar RT. Characterization of tannic acid- and gallic acid-functionalized single- and multiwalled carbon nanotubes and an in vitro evaluation of their antioxidant properties. *J Taibah Univ Med Sci.* 2016;11(5):469-77. <https://doi.org/10.1016/j.jtumed.2016.07.006>.
29. Neo YP, Ray S, Jin J, Gizdavic-Nikolaidis M, Nieuwoudt MK, Liu D, et al. Encapsulation of food grade antioxidant in natural biopolymer by electrospinning technique: A physicochemical study based on zein–gallic acid system. *Food Chem.*

- 2013; 136(2):1013-21. <https://doi.org/10.1016/j.foodchem.2012.09.010>.
30. Miyata Y, Mizuno K, Kataura H. Purity and defect characterization of single-wall carbon nanotubes using raman spectroscopy. *J Nanomater.* 2011; 2011(1):786763. <https://doi.org/10.1155/2011/786763>
31. López-Díaz D, López Holgado M, García-Fierro JL, Velázquez MM. Evolution of the Raman Spectrum with the Chemical Composition of Graphene Oxide. *J Phys Chem C.* 2017; 121(37):20489-97. <https://doi.org/10.1021/acs.jpcc.7b06236>
32. Fang S, Chen K, Yao H, Cao Y, Guo S, Wang L, et al. Preparation of gallic acid intercalated layered double hydroxide for enhanced corrosion protection of epoxy coatings. *Coatings.* 2023; 13(1): 128. <https://doi.org/10.3390/coatings13010128>.
33. Ramezanzadeh M, Ramezanzadeh B, Mahdavian M, Bahlakeh G. Development of metal-organic framework (MOF) decorated graphene oxide nanoplateforms for anti-corrosion epoxy coatings. *Carbon.* 2020; 161:231-51. <https://doi.org/10.1016/j.carbon.2020.01.082>.
34. Usman BJ, Umoren SA, Gasem ZM. Inhibition of API 5L X60 steel corrosion in CO<sub>2</sub>-saturated 3.5% NaCl solution by tannic acid and synergistic effect of KI additive. *J Mol Liq.* 2017; 237:146-56. <https://doi.org/10.1016/j.molliq.2017.04.064>.
35. Asperti D, Cabrini M, Lorenzi S, Rosace G, Omrani A, Pastore T. Electrochemical impedance spectroscopy analysis of organic epoxy coatings reinforced with nano clay. *Materials.* 2024; 17(12): 3028. <https://doi.org/10.3390/ma17123028>.
36. Yuan X, Du Y, Lin Z, Liu Z, Gu L. Effect of Water Uptake, Adhesion and anti-corrosion performance for silicone-epoxy coatings treated with GLYMO on 2024 Al-alloy. *Polymers.* 2022; 14(15): 3076. <https://doi.org/10.3390/polym14153076>.
37. Alhozaimy A, Hussain RR, Al-Negheimish A, Ahmed M, Singh DDN. Kinetics and mechanism of gallic acid as an ecofriendly corrosion inhibitor for steel rebars in mortar. *Sci Rep.* 2024; 14(1):31015. <https://doi.org/10.1038/s41598-024-82166-4>
38. Ramezanzadeh B, Rostami M, Niroumandrad S. Enhancement of the physical/mechanical properties of an epoxy composite by addition of aluminum nanoparticles through modification with cerium oxides and functionalization by

- SiO<sub>2</sub>-NH<sub>2</sub> thin films. Prog Org Coatings. 2017; 112:244-53.  
<https://doi.org/10.1016/j.porgcoat.2017.07.005>.
39. Zhen LIU, Yun YU, Menghang Z, Liuye YIN, Yufei D, Guixiang HOU. Curing kinetics and properties of gallic acid epoxy resin/ricinoleic acid- based polyamine thermosetting system. China Plast. 2022; 36(2):75.  
<https://doi.org/10.19491/j.issn.1001-9278.2022.02.012>.
40. Zhou Y, Xu G, Fan Y, Li Y, Chen X, Yang J, et al. Multi-objective toughness optimization of epoxy resin for steel bridge deck pavement based on crosslink density regulation. Polymers. 2025; 17(10): 1422.  
<https://doi.org/10.3390/polym17101422>.
41. Hou G, Li N, Han H, Run M, Gao J. Preparation and thermal properties of bio-based gallic acid epoxy/carbon nanotubes composites by cationic ring-opening reaction. Polym Compos. 2016; 37(10):3093-102.  
<https://doi.org/10.1002/pc.23507>
42. Senthilkumar G, Umarani C, Ramachandran A. Investigation on corrosion inhibition effect of N-[4-(1,3-benzo[d]thiazol-2-ylcarbamoyl)phenyl]quinoline-6-carboxamide as a novel organic inhibitor on mild steel in 1N HCl at different temperatures: Experimental and theoretical study. J Indian Chem Soc. 2021; 98(6):100079. <https://doi.org/10.1016/j.jics.2021.100079>.
43. Shah ST, A Yehya W, Saad O, Simarani K, Chowdhury Z, A. Alhadi A, et al. Surface functionalization of iron oxide nanoparticles with gallic acid as potential antioxidant and antimicrobial agents. Nanomaterials. 2017; 7(10):306  
<https://doi.org/10.3390/nano7100306>.
44. Levy L, Gurov A, Radian A. The effect of gallic acid interactions with iron-coated clay on surface redox reactivity. Water Res. 2020; 184:116190.  
<https://doi.org/10.1016/j.watres.2020.116190>.